Control of Lasing from Bloch States in Microcavity Photonic Wires via Selective Excitation and Gain

A. Mischok,* R. Brückner, H. Fröb, V. G. Lyssenko, and K. Leo
Institut für Angewandte Photophysik, Technische Universität Dresden, 01062 Dresden, Germany

A. A. Zakhidov†
Fraunhofer COMEDD, 01109 Dresden, Germany
(Received 26 March 2015; published 22 June 2015)

By adding photonic wire structures to an organic microcavity, we create an additional confinement and a Bloch-like band structure in the dispersion of periodically structured cavities. We experimentally observe spontaneous and stimulated emission from the ground and different excited discrete modes at room temperature. By changing the spatial gain distribution via a two-beam interference, we are able to directly control the laser emission from both extended and confined modes of such organic photonic wires. Both spatial distribution and dispersion exhibit coherent emission from tunable modes, which we describe with an analytical model and numerical simulations, in agreement with our measurements.

DOI: 10.1103/PhysRevApplied.3.064016

I. INTRODUCTION

Planar microcavities (MCs) have been under investigation since the early 1990s, both experimentally [1] and theoretically [2]. While for MCs in the weak-coupling regime, a parabolic cavity mode is observed, the formation of an upper and lower polariton branch has been observed more recently in GaAs [3,4] as well as organic [5] MCs in the regime of strong exciton-polariton coupling. Under high excitation (above threshold), cavity photons exhibit coherent behavior such as stimulated emission and spectral narrowing, while exciton polaritons have been shown to undergo phase transitions towards a macroscopic ground-state occupation described as Bose-Einstein condensation in the lower polariton branch [6,7]. In those cases, the coherent photons or polaritons emit from this mode under an in-plane wave vector $k = 0$ in the parabolic dispersion of the lower polariton branch or MC photon dispersion. Coherent emission from polaritons in non-ground-states was observed under resonant pumping explained by an incomplete polariton down-relaxation and their short lifetime. Coherent emission from excited states of planar MCs at resonant laser excitation has also been observed experimentally [8,9] and explained as the reemission of the excitation laser into a ringlike distribution in k space due to elastic resonant Rayleigh scattering at static disorder. Ring-shaped coherent emission at nonresonant excitation was reported [10] and explained in GaAs MCs where excess energy was lost before being captured into a bottleneck trap [9]. Ring-shaped coherent emission has further been observed in CdTe [11] and organic [12] MCs, due to scattering of light into multiple cavity modes at $k \neq 0$.

In both zero-dimensional (0D) and one-dimensional (1D) microstructures (i.e., photonic boxes [13] and photonic wires [14,15]), photon and polariton modes are confined within the micrometer-size volume. In this case, their continuous parabolic dispersion is transformed into a set of confined discrete states. Zero-dimensional confinement in the lateral plane has been demonstrated in different examples of cylindrical pillars [16,17], square [18] or elliptical [19,20] photonic boxes, and 1D confinement, for example, in photonic wires. Periodically arranged photonic wires offer a possibility of studying the formation of Bloch states in ZnO [21] or (Ga,Al)as MCs [22], showcasing coherent emission from nonground gap states in the Bloch-like polariton dispersion [23]. More recently, a Fibonacci-sequence pattern has been investigated by the same group [24]. Cerna *et al.* [25] demonstrated the manipulation of the spatial and angular distribution of confined polariton modes in a 0D pillar by tuning either the incidence angle of the excitation beam and/or its energy at below-threshold intensities. Moreover, optical structuring has been employed, where the formation of an exciton population in a particular pumping geometry locally increases the cavity potential and leads to emission from confined modes [26] or geometrical phase locking of emission from several excited spots [27,28]. Furthermore, gain-induced trapping of exciton polaritons has been utilized by Roumpos *et al.* [29] due to the short lifetime and finite size of excitations.

A manipulation of coherence in ground and excited states could be shown in circular pillars [30,31] and photonic wires [32,33] by a controlled shift of the excitation spot position. Furthermore, a switching of coherent

*andreas.mischok@iapp.de
†Present address: Texas State University, 601 University Drive, San Marcos, TX, USA.

modes was demonstrated by spatially selective excitation under nonresonant optical pumping in GaAs pillar MCs.

While a multitude of publications deal with inorganic systems, usually grown by highly involved molecular beam epitaxy, the investigation of organic active materials has recently shown interesting possibilities for low-threshold lasing, e.g., in patterned photonic crystals [34,35] or even Bose-Einstein condensation in a MC at room temperature [5]. Furthermore, the class of hybrid organic-inorganic perovskites promises interesting tunable laser applications in the future [36]—with the need for precise optical control.

Our work addresses the coherent emission of SiO_2 photonic wires in a MC with an organic active medium. Under spatially selective excitation, we show the possibility to precisely control the spectral and angular position of lasing from the wire and above the potential barrier. Numerical simulations accompany our experimental results to further showcase the effect of our selective gain distribution. Even though we work in the weak-coupling regime, our results are more generally applicable towards guiding, trapping, and controlling photons or polaritons in organic or inorganic MCs.

II. SAMPLE AND EXPERIMENTAL SETUP

We investigate MCs with a $\lambda_C/2$ cavity layer at the design wavelength λ_C, comprising 2% of the laser dye dicyanomethylene-2-methyl-6-*p*-dimethylaminostyryl-4*H*-pyran(DCM) doped into the matrix tris-(8-hydroxyquinolinato)-aluminum (Alq_3, $n_O \approx 1.75$). The broadband organic laser dye provides gain over a large spectral range [see Fig. 1(a)], enabling the direct investigation of the cavity dispersion as well as allowing tunable lasing in the system. This cavity is encased by two distributed Bragg reflectors (DBRs) with reflectivities $R \geq 99.5\%$ near the stop-band center at the cavity resonance $\lambda_C \approx 630$ nm and provides quality factors on the order of 1000 in free and confined areas alike. For 1D confinement in organic photonic wires with micron-size widths L_W from approximately 1 μm to approximately 10 μm, we utilize optical lithography to add thin SiO_2 stripes ($n_{SiO_2} = 1.45$) via a lift-off process. This patterning modulates the cavity thickness with an amplitude of $d_{SiO_2} = 15$ nm and periods of 3.71–4.8 μm. Figure 1(b) shows the cavity design with photonic wires consisting of the organic layer and additional SiO_2 stripes sandwiched between two similar DBRs. Each photonic wire is surrounded by barriers of only the organic cavity layer with a smaller height $d_O = \lambda_c/2n_O$ and width L_B approximately 2 μm to approximately 10 μm.

The DBRs are fabricated by reactive electron-beam evaporation of 21 alternating layers of TiO_2 and SiO_2 with quarter-wavelength thicknesses, under a base pressure of 5×10^{-7} mbar and a partial oxygen pressure of 2×10^{-4} mbar. On the bottom mirror, a commercial negative-tone photoresist (AZ nLOF 2020 by MicroChemicals) is spin coated and exposed through a

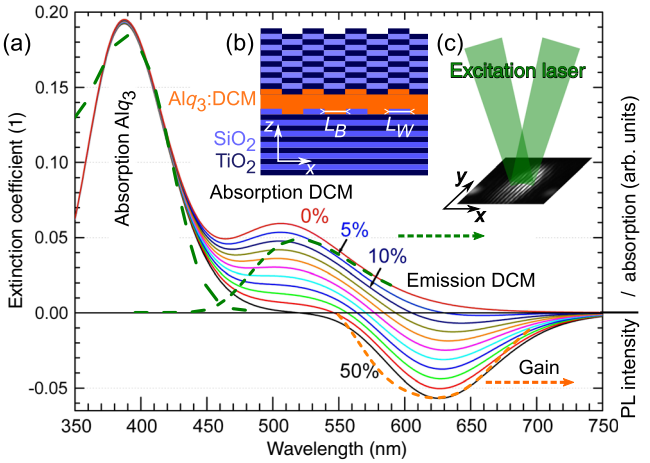

FIG. 1. (a) Calculated absorption spectra of the organic emitter system for different fractions of excited DCM molecules. Apart from the absorption of Alq_3 centered at 400 nm and the absorption of DCM at 510 nm, we see the occurrence of gain (negative absorption) around 630 nm, for higher fractions of excited molecules. Dashed lines: Measured absorption of pure Alq_3 and DCM (green); photoluminescence intensity of 2 wt % DCM in Alq_3 (orange). (b) Sample schematic. DBR mirrors contain an organic cavity with SiO_2 wires of width L_W and barriers of width L_B. (c) Excitation geometry for selective excitation. The pump beam is split into two beams, which interfere under an oblique angle of incidence and create a periodic distribution of gain in the sample plane.

contact mask with periodic stripe patterns of the different widths and periods presented. Following development, approximately 15 nm of SiO_2 is deposited on top and, after lift-off of the resist, yields the photonic wires. The active layer of Alq_3:DCM is deposited on top of this structure by thermal coevaporation of matrix and dye under a base pressure of 5×10^{-7} mbar. The thickness of this crucial cavity layer (physical thickness approximately 183 nm) is controlled by an *in situ* transmission measurement during evaporation. The samples are finished by a top DBR, similar to the first one. Because of the thermal evaporation of all layers, the patterning is continued to the top of the device [see schematic Fig. 1(b)] and creates the photonic confinement we observe in all near- and far-field figures.

For below- and above-threshold optical excitation of both wires and surrounding barriers, we use a pulsed solid-state laser (1.5 ns, 2 kHz, 532 nm) split into one or two beams and focused by a ×25 microscope objective into spots with diameters from 2 to 50 μm. The emission in the near or far field [37] is collected by a standard microscope objective ×63 (NA = 0.8) with an angular aperture of ±50°, sent into the entrance slit of a 0.6-m imaging spectrometer and recorded by a cooled charge-coupled device. All far-field spectra are recorded in TE polarization using a polarization filter in front of the detection setup. The high-quality samples and confocal microscope

objectives allow the detection of spatially and angle-resolved emission spectra even at room temperature. For a sketch of a similar microphotoluminescence setup, see, e.g., Lai *et al.* [38], Fig. 2(a).

The organic dyes we employ offer certain advantages in MC research and application. The calculated extinction coefficient in Fig. 1(a) shows the transformation of absorption into gain even for small percentages of excited DCM molecules. The absorption and emission spectra of evaporated Alq_3:DCM layers have been measured and published many times, including the net gain spectrum

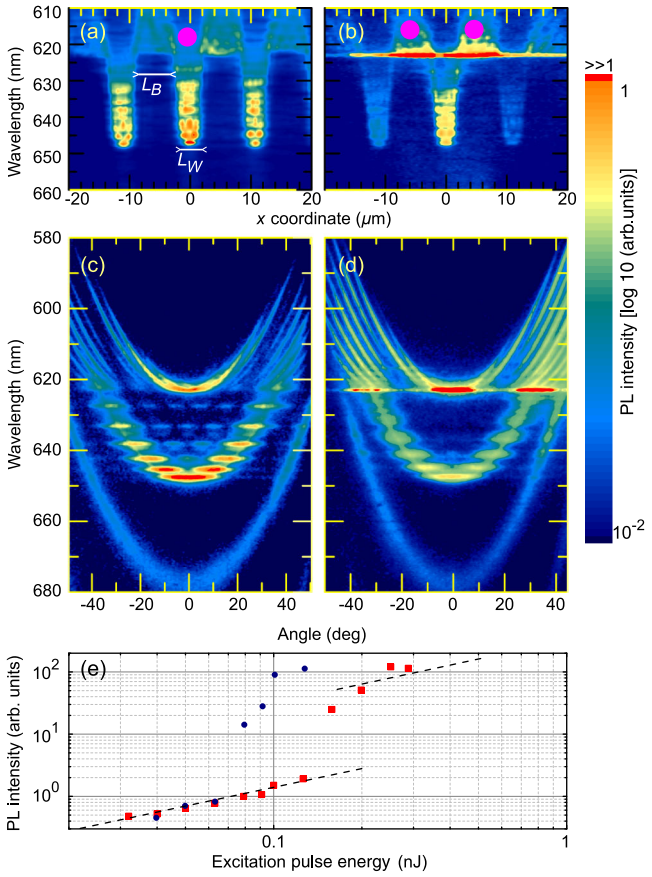

FIG. 2. (a),(b) Spatially resolved emission spectrum perpendicular to a photonic wire for above-threshold excitation localized on the wire [(a) $L_W = 3.7$ μm] and of the barrier [(b) $L_B = 7.4$ μm]. The potential induced by the SiO_2 wire laterally traps photons in discrete standing wave modes. Lasing takes place either from the lowest confined state (a) or the lowest extended above-barrier state (b) (deep red). The excitation spot position is indicated in pink. (c),(d) Angle-resolved emission corresponding to (a) and (b). The emission from the barrier exhibits a flat dispersion, while the above-barrier states show a Bloch-like dispersion with almost continuous spectra. The intensity is color coded in logarithmic scale in all figures. (e) Input-output curve for excitation of the barrier as in (b), (d) (red squares) with a lasing threshold of 0.15 nJ (approximately 20 $\mu J/cm^2$) and for the excitation of the wire as in (a), (c) (blue circles) with a threshold of 0.1 nJ. Dashed lines with a slope of 1 are added as a guide for the eye.

(e.g., Ref. [39]). From these data and our own experimentally obtained spectra, we estimate the oscillator strengths of the corresponding transitions per DCM molecule. An excitation of a fraction $N(P)/N(0)$ of the DCM molecules then proportionally decreases the absorption spectrum and increases the emission spectrum assuming roughly equal oscillator strengths, resulting in normalized absorption or net gain spectra with a maximum corresponding to approximately 60 cm^{-1} in the bare film [39]. At higher excitation, the organic system gives access to a gain spectrum spanning over 150 nm, allowing for tunable devices and direct observation of the full cavity emission spectrum in real and k space. The Frenkel excitons in small molecules exhibit large exciton binding energies in comparison to the Wannier-Mott excitons in inorganic semiconductors, which, on the one hand, drastically increase their stability and allow room-temperature experiments. On the other hand, the strong localization of the exciton provides a large oscillator strength as an ideal prerequisite for lasing application. We off resonantly excite either the Alq_3 matrix at 405 nm or the laser dye DCM at 532 nm, leading to the formation of a broad gain spectrum around 630 nm in a four-level system formed by the organic dyes in the weak-coupling regime.

III. RESULTS AND DISCUSSION

Microcavities exhibit a parabolic dispersion up to certain angles, above a constant potential determined by the cavity thickness. An additional thin layer of SiO_2 in our system causes a shift in the MC energy landscape; i.e., the photon potential is redshifted according to

$$E_{\mathrm{cav}} = \frac{\pi\hbar c}{n_O d_O + n_{\mathrm{SiO_2}} d_{\mathrm{SiO_2}}}, \tag{1}$$

where n_i and d_i are the refractive indices and physical thickness of the organic (O) cavity layer and the SiO_2 wires. Please note that this equation is an approximation that is valid near the center of the DBR stop band, where the penetration into neighboring mirror layers is minimal. A full calculation is found in Ref. [40]. In our photonic wires, this shift causes an index-guided confinement which discretizes the MC resonance into several standing wave modes exhibiting flat dispersion below the potential barrier. Both redshift and discretization are visible in the spatially resolved μ-photoluminescence measurement in Fig. 2(a). The low absorption of the 3.7-μm-wide wire and the high quality of patterning enable the direct observation of the spatial distribution of light from the ground state with one antinode to higher excited trapped states with up to six antinodes visible in the experiment (648–625 nm). Above the photonic-barrier potential, the dispersion is extended, with the appearance of photonic minibands (<623 nm). The angle-resolved dispersion in Fig. 2(c) shows the flat dispersion of confined states and their inner satellites. Here,

above the barrier, a multitude of Bragg-scattered extended states become visible, being repeated after each reciprocal lattice constant $2\pi/(L_W + L_B)$. Because of sample impurities and the local excitation of only one well, the photonic miniband structure is not well resolved here. Such a Bloch-like dispersion has been presented in metal photonic wires before [41].

A. Above-threshold investigation

For (far-) above-threshold excitation of the photonic wires, we observe two types of lasing depending on the positioning of the pump spot. While placing a single pump spot strongly focused over one photonic wire [marked as a pink circle in Fig. 2(a)], the coherent emission originates from the bottom of the potential well, at 648 nm and $k = 0$ [see Fig. 2(c)], where the parabola apex would appear in an unstructured MC. Shifting the excitation to the position of the barrier [Figs. 2(b) and 2(d); input-output curve 2(e)], the strong stimulated emission is now concentrated at 623 nm, as a supermode above the left and right barriers at ± 5 μm. In k space, we do not observe only the laser emission at zero angle but a strong scattering into the hybrid well-barrier state at angles $\pm 30°$ can be seen. An analogous behavior can be observed in the formation of a Kastler ring in MCs with multiple cavity modes [12]. The extended Bloch states are illuminated more strongly for an excitation of the barrier and show a first hint of the photon miniband structure.

Utilizing this spatially selective pump above threshold, we can manipulate the coherent emission from discrete states confined in separated excited photonic wires or from an extended Bloch wave propagating through excited barriers and neighboring nonexcited photonic wires.

While the gain profile of the organic Alq_3:DCM emitter system covers a broad spectral range, its peak is centered at 630 nm. Utilizing the flat dispersion in photonic wires, we are able to probe this distribution when exciting the wires only slightly above threshold. In Fig. 3, photonic wires of different widths $L_W = 1.0$, 3.7, and 10.0 μm exhibit coherent emission only at 630 nm $\pm$ 3 nm for a pump intensity at or slightly above the lasing threshold. The overall high density of photonic states allows lasing from non-ground-states, provided the peak gain value can overcome absorption which happens only in higher excited modes closer to the emission maximum. For larger excitation energies, the coherent emission shifts again towards the potential well or -barrier ground state, where the highest Q values are obtained.

B. Photonic Bloch states

All angle-resolved spectra here follow the same general sample composition, i.e., showing confined wire states at 648–625 nm, while the different widths of the potential well strongly influence the appearance and number of the discrete flat modes. The distribution of these states can be

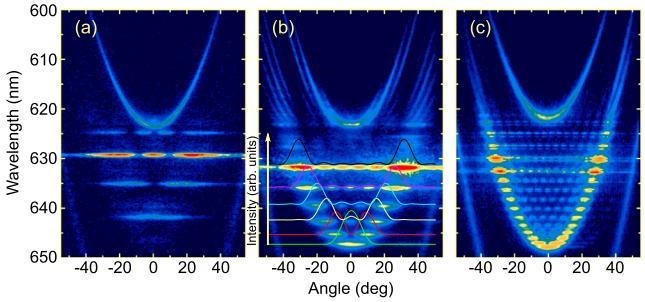

FIG. 3. Angle-resolved emission from photonic wire arrays of different $L_W = 1$ μm (a), 3.7 μm (b), and 10.0 μm (c) for excitation on the wire. The width of the photonic wire leads to a closer or wider spacing of the discrete modes below the barrier and a differing total number of confined states. Because of the flat dispersion of the confined states, lasing originates from the modes closest to the gain maximum of the organic emitter, even for different geometries. Intensity is color coded as in Fig. 2. Solid lines in (b) represent calculations of k spacing according to Eq. (4)

calculated using a modified Kronig-Penney model, where the particle energy and effective mass are substituted by their photonic counterparts in MCs [41]. For the approximation of high barriers, the spatial mode distribution $F_m(x)$ can then be expressed as

$$F_m(x) \approx \cos(q_m x) \quad \text{or} \quad \sin(q_m x). \tag{2}$$

Here, the discretized modes are labeled by an integer $m = 0, \pm 1, \pm 2, \ldots$, yielding the corresponding wave numbers $q_m = \pi(m+1)/L_W$. The energies of the modes are, furthermore, given by [18]

$$E_m = \pi\hbar c \sqrt{\frac{1}{(n_O d_O + n_{SiO_2} d_{SiO_2})^2} + \frac{(m+1)^2}{n_C^2 L_W^2}}, \tag{3}$$

with an effective cavity refractive index $n_C \approx f_O n_O + (1 - f_O) n_{SiO_2}$ and f_O the fraction of the organic layer in the cavity thickness. The analytical expression for the angular distribution (with $k_x \sin\theta$) of the emission intensity $I_m(k_x)$ follows from the Fourier transformation of the spatial distribution [42]:

$$I_m(k_x) \propto \cos\left(\frac{L_W k_x}{2} - \frac{m\pi}{2}\right)^2 \frac{q_m^2}{(q_m^2 - k_x^2)^2}. \tag{4}$$

This equation qualitatively yields the angle- and spectrally resolved emission of the discrete modes in the spectral range of 623 nm $< \lambda <$ 643 nm.

Even though the width of the photonic wire L_W does not influence the total redshift of the resonance [Eq. (1)], it has a significant influence on the number and spacing of the discrete modes, as apparent from Eqs. (3) and (4). Figure 3 showcases this behavior for the different widths of the

potential well on top of the photonic wires. Here, it becomes obvious that a smaller wire width leads to larger energetic gaps between and a smaller number of the discrete states. For imperfect sample conditions, i.e., a not perfectly square potential, the spectral position of modes differs. However, the k-space distribution after Eq. (4) still fits remarkably well, since the lateral confinement is very strong. This is showcased in Fig. 3(b) by solid lines.

C. Control of lasing by selective excitation

The spectral alignment of gain maximum and cavity modes, however, is not the only factor to consider. In particular, the spatial position and distribution of gain can have a significant impact on the spectral and angular distribution or even the threshold of laser emission in such photonic wires. If a strongly focused (<3 μm) excitation spot is centered exactly in a photonic wire, only symmetric (even) modes can overcome the threshold, while all antisymmetric (odd) modes show only weaker spontaneous emission. In general, the excitation reaches the highest efficiency when its spatial distribution overlaps with the corresponding field distribution of the laser mode. Utilizing this principle, we investigate the dependence of the near- and far-field emission spectra on spatially selective excitation of photonic wires. When the excitation spot at above-threshold intensity is focused into the center of the wire [see Fig. 4(a)], coherent emission emerges from the center of the excited wire with a wavelength $\lambda_0 = 643$ nm at $k = 0$. The remaining higher modes are still visible in spontaneous emission with significantly weaker intensity.

In our approximation (2), the confined modes have a periodic modulation with a period $P = 2L_W/(m+1)$ within a wire of the thickness L_W. For an optimal selective excitation of the mth confined mode, we split the pump laser beam into two and utilize the interference pattern created by focusing those two beams onto the sample under an oblique angle [see Fig. 1(c)]. This excitation geometry creates the desirable periodic population of excitons in the DCM and provides gain in the photonic wire that selectively excites certain modes. By changing the incident angles of the two excitation beams, the period of the interference pattern changes accordingly, allowing us to precisely control the excitation geometry in the system and to create standing waves with a distinct transversal wave number q_m. This way, the occurrence of coherent emission can be switched from the wire ground state [Figs. 4(a) and 4(e)] to higher excited states. To demonstrate this concept, we exemplarily show laser emission from modes $m = 1$ [Figs. 4(b) and 4(f)], $m = 5$ [Figs. 4(c) and 4(g)], and $m = 11$ [Figs. 4(d) and 4(h)]. Here, the micrographs Figs. 4(e)–4(h) show the near-field emission of the confined modes in the photonic wires, where we observe m nodes and $m+1$ antinodes in the spatially resolved emission of the respective state. Each mode is optimized for the lowest threshold of the nonresonant excitation. We are able not only to energetically tune the laser, but we can also directly control the main peak in the angular distribution of the coherent emission from $k = 0$ in the ground state over angles of $\pm 5°$ ($m = 1$), $\pm 14°$ ($m = 5$), and $\pm 23°$ ($m = 11$) to even higher angles. The satellite maxima of the higher excited states also provide an outcoupled laser light at exactly (for m even) or close to (for m odd) $k = 0$. The interference angles between the exciting beams outside of the cavity are approximately 10° [$m = 1$, Fig. 4(b)], approximately 31° [$m = 5$, Fig. 4(c)], and approximately 66° [$m = 11$, Fig. 4(d)]. The weak emission centered around (645 nm, +25°) is an artifact of the optical setup. We utilize the broadband emission of the laser dye and a fine control over the spatial exciton distribution via our pump scheme to allow for the experimental demonstration of the tunability in our system. As the tunability of the system stems mainly from the confinement of the wires, an application towards strong coupling is straightforward by substituting the luminescent dye for a system with sufficiently strong and narrow absorption in the spectral region of interest. This prospect will further open up fascinating new experiments such as spin optics, the investigation of magnetic properties, and propagation of excitons in such potential landscapes.

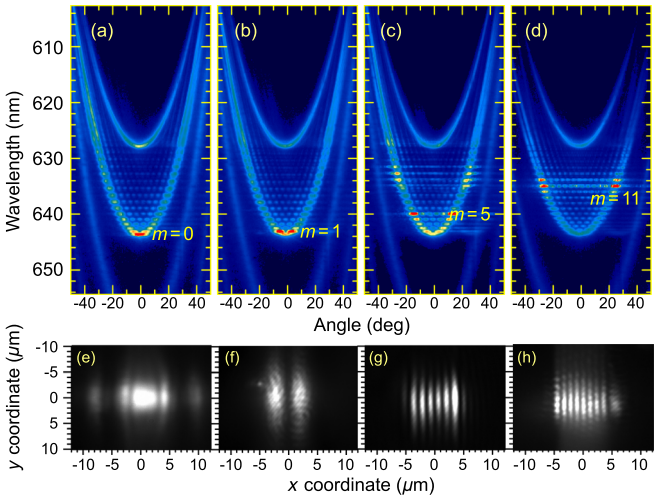

FIG. 4. Lasing from a photonic wire of $L_W = 10.0$ μm for different gain distributions created via two excitation-beam interference. (a)–(d) show the angle-resolved dispersion, while (e)–(h) show the corresponding modes in the near field. Here, the x coordinate is perpendicular, while the y coordinate is parallel to the wire orientation. By varying the angle of two excitation beams and, thus, the spatial distribution of gain, modes with a corresponding field distribution are selectively excited from the ground state with one antinode (a) to higher excited states with $m+1$ antinodes (b)–(d). Intensity in (a)–(d) is color coded as in Fig. 2.

D. Numerical simulation

To quantitatively confirm our experimental spectra, we numerically simulate the emission from a periodic

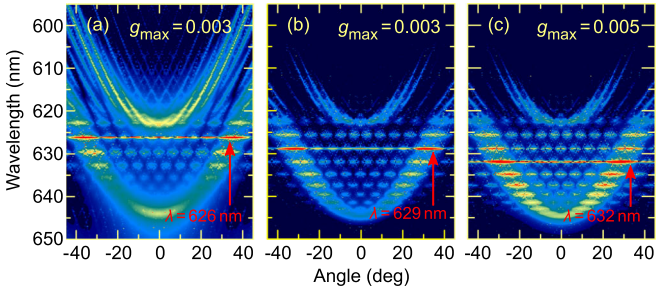

FIG. 5. Calculated angle-resolved spectra of emission from photonic wires under different gain distributions. Intensity is color coded as in Fig. 2.

($P = 10\ \mu$m) array of photonic wires with a width of $L_W = 5\ \mu$m using a rigorous coupled wave analysis. In the angle-resolved image presented in Fig. 5, we again confirm the coexistence of confined and extended Bloch states below and above the potential barrier of the SiO_2 wires. As the simulation assumes a perfect sample condition, we can also observe the Bloch-like photonic miniband structure above the barrier here.

In our approach, the amplitude and spectral shape of gain is taken into consideration, both dependent on excitation intensity. For the simulation, we create an excitation array of different spatially distributed gain maxima amplitudes: $g_{\max}(626\,\text{nm}) = 3\times10^{-3}$ Fig. 5(a), $g_{\max}(629\,\text{nm}) = 3\times10^{-3}$ Fig. 5(b), and $g_{\max}(631\ \text{nm}) = 5\times10^{-3}$ Fig. 5(c). As marked in red, lasing starts from the confined modes that closely resemble the spatial gain distribution. The wavelength and angular distribution of coherent emission can be easily tuned by switching between different confined modes utilizing our excitation scheme.

IV. CONCLUSION

In a photonic wire microcavity, we realize the one-dimensional confinement of photons in a photonic potential well created by stripes of SiO_2. We experimentally observe photonic Bloch states as a spectral discretization of the cavity dispersion below and extended quasicontinuous states above the confining potential and are able to describe these modes via a Kronig-Penney model tailored to our system. Using a broadband organic emitter, we directly probe its gain distribution in differently sized wires with flat dispersion. By creating a spatial distribution of excitons in our pump scheme, we take advantage of the wide spectral range of the emitter and directly tune the laser emission from the ground state at $k = 0$ to arbitrarily high excited states at smaller wavelengths and larger outcoupling angles. Therefore, our finely tuned experimental conditions enable us to directly control the coherent emission in the device. A numerical simulation confirms our measurement and provides further insight into the photonic band structure above the wire potential.

ACKNOWLEDGMENTS

The authors gratefully acknowledge financial support from the German Bundesministerium für Bildung und Forschung through the InnoProfile Project (Project No. 03IP602), the DFG Projects No. LE 747/37-1 and No. LE747/41-1, and via the excellence cluster cfaed. A. M. acknowledges support from the European Social Fund via the OrganoMechanics Project and the European Union for funding under the 7th Framework Programme, Project NUDEV (Project No. FP7-267995). A. A. Z. acknowledges support as a fellow of the Humboldt Foundation.

[1] C. Weisbuch, M. Nishioka, A. Ishikawa, and Y. Arakawa, Observation of the Coupled Exciton-Photon Mode Splitting in a Semiconductor Quantum Microcavity, Phys. Rev. Lett. **69**, 3314 (1992).

[2] G. Bjork, S. Machida, Y. Yamamoto, and K. Igeta, Modification of spontaneous emission rate in planar dielectric microcavity structures, Phys. Rev. A **44**, 669 (1991).

[3] R. Houdre, C. Weisbuch, R. P. Stanley, U. Oesterle, P. Pellandini, and M. Ilegems, Measurement of Cavity-Polariton Dispersion Curve from Angle-Resolved Photoluminescence Experiments, Phys. Rev. Lett. **73**, 2043 (1994).

[4] E. Peter, P. Senellart, D. Martrou, A. Lemaître, J. Hours, J. M. Gérard, and J. Bloch, Exciton-Photon Strong-Coupling Regime for a Single Quantum Dot Embedded in a Microcavity, Phys. Rev. Lett. **95**, 067401 (2005).

[5] J. D. Plumhof, T. Stöferle, L. Mai, U. Scherf, and R. F. Mahrt, Room-temperature Bose-Einstein condensation of cavity exciton-polaritons in a polymer, Nat. Mater. **13**, 247 (2014).

[6] F. Boeuf, R. André, R. Romestain, Le Si Dang, E. Péronne, J. F. Lampin, D. Hulin, and A. Alexandrou, Evidence of polariton stimulation in semiconductor microcavities, Phys. Rev. B **62**, R2279 (2000).

[7] C. Schneider, A. Rahimi-Iman, N. Young Kim, J. Fischer, I. G. Savenko, M. Amthor, M. Lermer, A. Wolf, L. Worschech, V. D. Kulakovskii, I. A. Shelykh, M. Kamp, S. Reitzenstein, A. Y. Yamamoto, and S. Höfling, An electrically pumped polariton laser, Nature (London) **497**, 348 (2013).

[8] T. Freixanet, B. Sermage, J. Bloch, J. Y. Marzin, and R. Planel, Annular resonant Rayleigh scattering in the picosecond dynamics of cavity polaritons, Phys. Rev. B **60**, R8509 (1999).

[9] R. Houdre, C. Weisbuch, R. P. Stanley, U. Oesterle, and M. Ilegems, Coherence effects in light scattering of two-dimensional photonic disordered systems: Elastic scattering of cavity polaritons, Phys. Rev. B **61**, R13333(R) (2000).

[10] P. G. Savvidis, J. J. Baumberg, D. Porras, D. M. Whittaker, M. S. Skolnick, and J. S. Roberts, Ring emission and exciton-pair scattering in semiconductor microcavities, Phys. Rev. B **65**, 073309 (2002).

[11] M. Richard, J. Kasprzak, R. Romestain, R. André, and Le Si Dang, Spontaneous Coherent Phase Transition of

Polaritons in CdTe Microcavities, Phys. Rev. Lett. **94**, 187401 (2005).

[12] P. Schneeweiss, M. Sudzius, R. Gehlhaar, M. Hoffmann, V. G. Lyssenko, H. Fröb, and K. Leo, Observation of Kastler ring stimulated emission from an organic microcavity, Appl. Phys. Lett. **91**, 051118 (2007).

[13] O. El Daïf, A. Baas, T. Guillet, J.-P. Brantut, R. Idrissi Kaitouni, J. L. Staehli, F. Morier-Genoud, and B. Deveaud, Polariton quantum boxes in semiconductor microcavities, Appl. Phys. Lett. **88**, 061105 (2006).

[14] A. I. Tartakovskii, V. D. Kulakovskii, A. Forchel, and J. P. Reithmaier, Exciton-photon coupling in photonic wires, Phys. Rev. B **57**, R6807 (1998).

[15] A. Mischok, F. Lemke, C. Reinhardt, R. Brückner, A. A. Zakhidov, S. I. Hintschich, H. Fröb, V. G. Lyssenko, and K. Leo, Dispersion tomography of an organic photonic-wire microcavity, Appl. Phys. Lett. **103**, 183302 (2013).

[16] J. M. Gérard, B. Sermage, B. Gayral, B. Legrand, E. Costard, and V. Thierry-Mieg, Enhanced Spontaneous Emission by Quantum Boxes in a Monolithic Optical Microcavity, Phys. Rev. Lett. **81**, 1110 (1998).

[17] C. Schneider, T. Heindel, A. Huggenberger, T. A. Niederstrasser, S. Reitzenstein, A. Forchel, S. Höfling, and M. Kamp, Microcavity enhanced single photon emission from an electrically driven site-controlled quantum dot, Appl. Phys. Lett. **100**, 091108 (2012).

[18] J. P. Reithmaier, M. Röhner, H. Zull, F. Schäfer, A. Forchel, P. A. Knipp, and T. L. Reinecke, Size Dependence of Confined Optical Modes in Photonic Quantum Dots, Phys. Rev. Lett. **78**, 378 (1997).

[19] B. Gayral, J. M. Gérard, B. Legrand, E. Costard, and V. Thierry-Mieg, Optical study of GaAs/AlAs pillar microcavities with elliptical cross section, Appl. Phys. Lett. **72**, 1421 (1998).

[20] A. Mischok, R. Brückner, M. Sudzius, C. Reinhardt, V. G. Lyssenko, H. Fröb, and K. Leo, Photonic confinement in laterally structured metal-organic microcavities, Appl. Phys. Lett. **105**, 051108 (2014).

[21] L. Zhang, W. Xie, J. Wang, A. Poddubny, J. Lu, Y. Wang, J. Gu, W. Liu, D. Xu, X. Shen, Y. G. Rubo, B. L. Altshuler, A. V. Kavokin, and Z. Chen, Weak lasing in one-dimensional polariton superlattices, Proc. Natl. Acad. Sci. U.S.A. **112**, E1516 (2015).

[22] K. Winkler, J. Fischer, A. Schade, M. Amthor, R. Dall, J. Gessler, M. Emmerling, E. A. Ostrovskaya, M. Kamp, C. Schneider, and S. Höfling, A polariton condensate in a photonic crystal potential landscape, New J. Phys. **17**, 023001 (2015).

[23] D. Tanese, H. Flayac, D. Solnyshkov, A. Amo, A. Lemaître, E. Galopin, R. Braive, P. Senellart, I. Sagnes, G. Malpuech, and J. Bloch, Polariton condensation in solitonic gap states in a one-dimensional periodic potential, Nat. Commun. **4**, 1749 (2013).

[24] D. Tanese, E. Gurevich, F. Baboux, T. Jacqmin, A. Lemaître, E. Galopin, I. Sagnes, A. Amo, J. Bloch, and E. Akkermans, Fractal Energy Spectrum of a Polariton Gas in a Fibonacci Quasiperiodic Potential, Phys. Rev. Lett. **112**, 146404 (2014).

[25] R. Cerna, D. Sarchi, T. K. Paraïso, G. Nardin, Y. Léger, M. Richard, B. Pietka, O. El Daif, F. Morier-Genoud, V. Savona, M. T. Portella-Oberli, and B. Deveaud-Plédran, Coherent optical control of the wave function of zero-dimensional exciton polaritons, Phys. Rev. B **80**, R121309 (2009).

[26] A. Dreismann, P. Cristofolini, R. Balili, G. Christmann, F. Pinsker, N. G. Berloff, Z. Hatzopoulos, P. G. Savvidis, and J. J. Baumberg, Coupled counterrotating polariton condensates in optically defined annular potentials, Proc. Natl. Acad. Sci. U.S.A. **111**, 8770 (2014).

[27] G. Tosi, G. Christmann, N. G. Berloff, P. Tsotsis, T. Gao, Z. Hatzopoulos, P. G. Savvidis, and J. J. Baumberg, Geometrically locked vortex lattices in semiconductor quantum fluids, Nat. Commun. **3**, 1243 (2012).

[28] R. Brückner, A. A. Zakhidov, R. Scholz, M. Sudzius, S. I. Hintschich, H. Fröb, V. G. Lyssenko, and K. Leo, Phase-locked coherent modes in a patterned metalorganic microcavity, Nat. Photonics **6**, 322 (2012).

[29] G. Roumpos, W. H. Nitsche, S. Höfling, A. Forchel, and Y. Yamamoto, Gain-Induced Trapping of Microcavity Exciton Polariton Condensates, Phys. Rev. Lett. **104**, 126403 (2010).

[30] D. Bajoni, P. Senellart, E. Wertz, I. Sagnes, A. Miard, A. Lemaître, and J. Bloch, Polariton Laser Using Single Micropillar GaAs-GaAlAs Semiconductor Cavities, Phys. Rev. Lett. **100**, 047401 (2008).

[31] M. Maragkou, A. J. D. Grundy, E. Wertz, A. Lemaître, I. Sagnes, P. Senellart, J. Bloch, and P. G. Lagoudakis, Spontaneous nonground state polariton condensation in pillar microcavities, Phys. Rev. B **81**, 081307(R) (2010).

[32] E. Wertz, L. Ferrier, D. D. Solnyshkov, R. Johne, D. Sanvitto, A. Lemaître, I. Sagnes, R. Grousson, A. V. Kavokin, P. Senellart, G. Malpuech, and J. Bloch, Spontaneous formation and optical manipulation of extended polariton condensates, Nat. Phys. **6**, 860 (2010).

[33] L. Ferrier, E. Wertz, R. Johne, D. D. Solnyshkov, P. Senellart, I. Sagnes, A. Lematre, G. Malpuech, and J. Bloch, Interactions in Confined Polariton Condensates, Phys. Rev. Lett. **106**, 126401 (2011).

[34] P. B. Deotare, T. S. Mahony, and V. Bulović, Ultracompact low-threshold organic laser, ACS Nano **8**, 11080 (2014).

[35] B. Zhen, S.-L. Chua1, J. Lee, A. W. Rodriguez, X. Liang, S. G. Johnson, J. D. Joannopoulos, M. Soljačić, and O. Shapira, Enabling enhanced emission and low-threshold lasing of organic molecules using special Fano resonances of macroscopic photonic crystals, Proc. Natl. Acad. Sci. U.S.A. **110**, 13711 (2013).

[36] G. Xing, N. Mathews, S. S. Lim, N. Yantara, X. Liu, D. Sabba, M. Grtzel, S. Mhaisalkar, and T. C. Sum, Low-temperature solution-processed wavelength-tunable perovskites for lasing, Nat. Mater. **13**, 476 (2014).

[37] M. Richard, J. Kasprzak, R. Romestain, R. André, and Le Si Dang, Spontaneous Coherent Phase Transition of Polaritons in CdTe Microcavities, Phys. Rev. Lett. **94**, 187401 (2005).

[38] C. W. Lai, N. Y. Kim, S. Utsunomiya, G. Roumpos, H. Deng, M. D. Fraser, T. Byrnes, P. Recher, N. Kumada, T. Fujisawa, and Y. Yamamoto, Coherent zero-state and pi-state in an exciton-polariton condensate array, Nature (London) **450**, 529 (2007).

[39] S. Riechel, Ph.D. dissertation, Ludwig Maximilian University of Munich, 2002.

[40] G. Panzarini, L. C. Andreani, A. Armitage, D. Baxter, M. S. Skolnick, V. N. Astratov, J. S. Roberts, A. V. Kavokin, M. R. Vladimirova, and M. A. Kaliteevski, Exciton-light coupling in single and coupled semiconductor microcavities: Polariton dispersion and polarization splitting, Phys. Rev. B **59**, 5082 (1999).

[41] A. Mischok, V. G. Lyssenko, R. Brückner, F. Löchner, A. A. Zakhidov, H. Fröb, and K. Leo, Zero-and π-states in a periodic array of deep photonic wires, Adv. Opt. Mater. **2**, 746 (2014).

[42] T. Gutbrod, M. Bayer, A. Forchel, P. A. Knipp, T. L. Reinecke, A. Tartakovskii, V. D. Kulakovskii, N. A. Gippius, and S. G. Tikhodeev, Angle dependence of the spontaneous emission from confined optical modes in photonic dots, Phys. Rev. B **59**, 2223 (1999).